# COMPARISON OF NANOTUBES PRODUCED BY FIXED BED AND AEROSOL CVD METHODS AND THEIR ELECTRICAL PERCOLATION BEHAVIOUR IN MELT MIXED POLYAMIDE 6.6 COMPOSITES

B. Krause[a], M. Ritschel[b], Ch. Täschner[b], S. Oswald[b], W. Gruner[b], A. Leonhardt[b] , P. Pötschke[a*]

[a]Leibniz Institute of Polymer Research Dresden (IPF), Hohe Str. 6, 01069 Dresden, Germany

[b]Leibniz Institute for Solid State and Materials Research Dresden (IFW), P.O. Box 270116, 01171 Dresden, Germany

*corresponding author: Tel.: +49 3514658395; fax: +49 3514658565; poe@ipfdd.de

**Abstract**

We have investigated the percolation behaviour of different kinds of carbon nanotubes (CNTs) synthesised by two CVD techniques in an insulating polyamide 6.6 matrix incorporated by melt mixing. It was found that the electrical percolation behaviour depends strongly on the properties of CNTs. The lowest electrical percolation threshold (<0.1 wt%) was determined for as grown multi-walled carbon nanotubes (diameter approx. 20 nm) without any chemical treatment or purification. Such carbon nanotubes were synthesised by the aerosol-method and show relatively low oxygen content near the surface (XPS-measurements). In addition, nitrogen doped multi-walled nanotubes ($CN_x$) revealed also excellent electrical percolation behaviour with a similarly low percolation threshold.

Keywords: A. Carbon nanotubes, polymer-matrix composites; B. electrical properties, D. Optical microscopy, Scanning electron microscopy (SEM)

## 1. Introduction

In the recent past intense research has been carried out concerning the fabrication, characterisation, and application of polymer - carbon nanotube composites, driven by the unique mechanical, electrical and other material-related properties of carbon

nanotubes (CNTs) and the possibility of their mass production [1-3]. For instance, such composite materials based on conductive CNTs and insulating polymers are potential candidates for electrostatic dissipative or conductive applications, i.e. in the automotive engineering for the substitution of metal based car bodies.

Especially, already very small amounts of CNTs can induce significant changes of the polymer properties. In general, by addition of multi-wall CNTs (MWCNTs) into insulating polymers using melt-mixing electrical percolation thresholds in the range between 1 and 5 wt% CNTs are reported [4-6]. For further optimization of material properties it is desired to reduce the amount of CNT needed to get electrical percolation by retaining or enhancing most of the other properties of the polymer matrix.

The electrical percolation behaviour is mainly determined by the properties of the carbon nanotubes themselves (dimension, crystallinity, surface state, conductivity), by their dispersability in the polymer, and by the processing conditions during incorporation of CNTs in the polymer as well as the shaping steps. Whereas the properties of CNTs are already significantly contingent on the used synthesis process (e.g. CVD or laser ablation), the dispersion behaviour in the polymer additionally depends on the interactions between the nanotubes and the polymer. These interactions will be mainly determined by the chemical as-is state (polar, non-polar) of the tube surface (in as grown or functionalised state) and the polymer chains.

In this paper we compare differently synthesised CNT and report an unusual low percolation threshold of carbon nanotubes synthesised by an aerosol-CVD process in polyamide 6.6. On the other hand, carbon nanotubes fabricated by a so-called fixed bed method percolate at higher nanotube concentrations in the same polymers. The reasons of this different behaviour will be discussed.

## 2. Methods and Material

The synthesis of the CNTs was done using the catalytic CVD with two different CVD-techniques: the fixed bed method [7-12] and the aerosol method [13-17].

In the first case, a solid catalyst material is filled into a quartz boat and located in the hot zone of a CVD tube-reactor. The catalyst material consists of an active metal (Fe-nanoparticles and an admixture of Mo as promoter) deposited on magnesium oxide (MgO) powder [7, 18] and was prepared by a combustion reaction [19] of Mg- and Fe-nitrate and ammonium molybdate with citric acid as foaming and combustion additive

in deionised water [11]. The iron content in the catalyst material was varied to be 1, 4, 16 at%. This suspension was transferred directly into a furnace (560°C, air), where it spontaneously burned to MgO, Fe- and Mo-oxides (combustion product). A following reduction of this product was performed at a temperature of 600°C for 30 min in hydrogen. Metallic Fe- and Mo-particles were formed on the porous hard-to-reduce MgO powder (the so-called reduction product). Subsequently, during the injection of methane ($CH_4$) into the same reactor the temperature was increased to 1000°C and was maintained for 10 min. Afterwards, the $CH_4$-flow was stopped and the reactor in argon was cooled down. In order to remove the catalyst material the as-grown products were sonicated in a 1:1 hydrochloric acid /water mixture for 1h (50ml/g as grown product), filtered by PTFE-filter (0.45µm pores size), washed in distilled water, and finally dried at 110°C. Neither Mg by EDX- nor MgO by x-ray analysis could be detected after this procedure, respectively.

The aerosol technology is based on the injection of a solution (e.g. ferrocene saturated in organic solvents) in a furnace as an aerosol, generated by an ultrasonic unit (transducer). As transport gas a mixture of $Ar/H_2$ was used [13]. In the reaction zone of furnace (T between 700 and 900°C) the solution vaporizes and decomposed spontaneously and forms the CNTs. As solvents acetonitrile or cyclohexane were used both with a ferrocene concentration of 30 mg per ml solvent. The CVD equipment consists of a 1 m long quartz tube (diameter 40 mm) and a movable furnace (back and forth drive). In a typical procedure the total gas flow was kept at 1300 standard cubic centimetres per minute (sccm). During the synthesis process the furnace can be moved back and forth with a constant speed of few millimetres per minute. After the deposition process and cooling down of the reactor the synthesised CNTs could be easily scraped from the inserted tubes without any wet-chemical assistance. In this manner approx. 5 g CNTs with high purity were synthesised per experiment. The synthesised material contains only CNTs and can be followed up without any chemical treatment.

Analytical SEM (FEI-NOVA-NANO-SEM-200) and TEM (FEI Tecnai F30) investigations have been performed in order to characterize the CNTs (diameter, , number of shells, structure). For a statistical analysis of the diameter about 200 CNTs were observed. EDX-spectroscopy was used for element analysis (EDAX-system). X-ray photoelectron spectroscopy (XPS) measurements have given information about the

chemical constitution of the surface of the CNTs. For this a PHI 5600 CI (Physical Electronics) system equipped with a hemispheric energy analyser (pass energy of 29 eV, analysis region 800 µm in diameter) was applied. Monochromatised Al-Kα radiation was used for the excitation. The samples were agglomerated to a size of approx. 2x2x2mm$^3$ starting from randomly distributed tubes.

The chemical composition of the CNT starting materials was measured by different analytical methods that took into account the different syntheses aspects. The carrier gas hot extraction (CGHE) method using an Oxygen/Nitrogen analyser TC 436DR (Leco) was applied for determination of the oxygen and nitrogen content and using a hydrogen analyzer EMGA 621W (Horiba) for the analysis of organic residuals. The main carbon content was analysed by a combustion method using a carbon/sulphur analyser EMIA 820 (Horiba). Additionally, various other elements coming from the fixed bed support (Mg, Al) and/or the used catalysts (Fe, Co, Mo, e.g.) were checked by mass spectrometry and quantitatively measured by inductively coupled plasma-optical emission spectrometry (ICP-OES) method (IRIS XUV, Thermo). The obtained CNTs were also characterized using Raman spectroscopy and measurements of the specific surface area (BET).

For the preparation of the polymer based composites, powder of polyamide 6.6 (PA6.6, VYDYNE, Solutia Inc., Belgium) with a melt flow index of 600 g/10 min (275°C, 5 kg, ASTM Test Method D1238) and the CNTs synthesised as discussed above were vacuum-dried, dry-premixed, and melt mixed using a DACA microcompounder (DACA Instruments, Santa Barbara, USA) at 280°C and 50 rpm for 5 min. The selection of the processing temperature of 280°C was based on a former study [6] in which that temperature resulted in the lowest electrical resistivity values; the selection of 50 rpm resulted from results obtained by variation of the mixing speed on PA6. The short mixing time was selected in order to approximate usual mixing times during twin-screw extrusion. The viscosity vs. oscillation frequency values of that PA6.6 at 280°C are shown in ref. [6] and lie between 350 and 115 Pas at 0.04 and 100 rad/s, respectively.. A piece of the extruded strand with a diameter of 2 mm was pressed at 320°C for 2 min at 50 kN between two aluminium sheets to a thin plate with a thickness of approx. 0.3 mm and a diameter of 30 mm. The pressing conditions were optimized in pre-investigations to result in high conductivity values. To perform electrical conductivity measurements rectangular samples (30x4x0.3 mm$^3$) were cut from the pressed plates. For measuring, a

4-point test fixture (gold contact wires with a distance of 16 mm between the source electrodes and 10 mm between the measuring electrodes) combined with a Keithley electrometer E6517A was used. For conductivity values below $10^{-7}$ S/cm a Keithley 8009 Resistivity Test Fixture based on ring electrodes was used to measure the as pressed round plates.

Scanning electron microscopy (SEM) of the composite materials was performed using a LEO 435 (Carl-Zeiss AG Oberkochen, Germany). The composite strands were cryofractured in liquid nitrogen and the surfaces were observed after gold sputtering. The samples for light microscopy (LM) in transmission mode were cut from the extruded strands using a microtome Leica 2055 (Leica Mikrosysteme Vertrieb GmbH, Bensheim, Germany) to thin sections with a thickness of 10 µm and were fixed with Entellan® (Merck KGaA, Darmstadt, Germany) on glass slides. The light microscopy investigations were performed using a microscope BH2 and a camera DP71 (Olympus Deutschland GmbH, Hamburg, Germany) using different magnifications. The agglomerate area was quantified using an image analysis program Scandium (Olympus Soft Imaging Solutions GmbH, Münster, Germany) and related to the investigated area, for which in summary an area of about 3.6 $mm^2$ was evaluated.

## 3. Results

### 3.1. Synthesis and characterization of CNT

By using the fixed bed method for the CNT synthesis the experiments were performed with different iron-contents in the catalyst material. The influence of the iron-content on the structure of synthesised nanotubes is characterised by Figures 1 and 2. Figure 1 a shows a typical and representative MWCNT structure (resulting from extensive TEM-investigations) from the charge synthesised at high concentration of iron (16 at%) with outer tube diameters between 15 and 25 nm and about 20 graphitic carbon shells. The surface area of this charge determined by BET measurements is around 300 $m^2/g$. The results clearly indicate that at a middle iron concentration (4 at%) mixtures of MWCNT with diameters between 4 and 15 nm having 5-8 carbon shells and DW/SWCNT are generated (Figure 1 b, c). The relation of MWCNTs to DWCNTs and SWCNTs (DW/SWCNTs) quantities is approximately 50 to 50. The BET value of this charge increases to around 600 $m^2/g$.

The charge containing 1 at% Fe in the reduction material is characterized by a dominant amount of DWCNTs and SWCNTs (Figure 2) besides few very thin MWCNTs having 4 to 8 nm in diameter and circa 3-6 C-shells. The BET value of this charge was around 1050 $m^2/g$. It should to be noticed that both the DWCNTs and SWCNTs tend to the formation of bundles.

As already mentioned, before further processes the fixed bed-CNT have to be purified by washing in acids to remove the catalyst support (MgO). It is well known that such chemical treatment changes the surface of the CNTs via formation of functional groups as OH and COOH, which could be identified by different spectroscopical methods [20]. Also, the fixed bed-CNTs often possess amorphous C-deposits on the tube surface which decrease their electrical conductivity.

The aerosol-CVD method under the above mentioned conditions delivers only MWCNTs. However, the structure of CNTs is strongly dependent on the applied solvent. By using cyclohexane CNTs with a typical tubular structure (Figure 3 a) and a relatively high number of carbon-shells (up to 50 shells) have been synthesised. Otherwise, the application of acetonitrile as solvent leads to CNTs with a well-developed bamboo-like structure (Figure 3 b), which may be caused by the nitrogen incorporation into the shell structure [21-23]. In this case the number of shells is essentially lower (in generally between 4 and 10 shells).

The outer diameter of the MWCNTs (solvent: cyclohexane) ranges from 10 to 80 nm (Figure 4 a), the inner diameter from 10 to 20 nm. The nitrogen-doped MWCNTs (solvent: acetonitrile) have outer diameters between 8 and 40 nm (Figure 4 b), the inner diameters vary from 4 to 25 nm. Whereas the fixed bed-CNTs are often deposited with amorphous coatings, the surface of the aerosol-CNTs is extremely clean and does not show extrinsic depositions.

In Table 1 the results of the chemical analysis of three various CNT-types are shown:

CNT type A: fixed bed-CNTs with 4 at% Fe; SW/DW- and MWCNTs mixture.

CNT type B: aerosol-CNTs (solvent cyclohexane); tubular MWCNTs.

CNT type C: aerosol-CNTs (solvent acetonitrile); bamboo-like MWCNTs.

The chemical analyses of the various CNT types reflect directly the synthesis conditions. CNTs type A shows relatively high oxygen concentrations compared with the CNT types B and C that is caused by the acid treatment. When using acetonitrile as

solvent in the aerosol-CVD process CNTs with an increased nitrogen concentration were produced.

While the chemical analysis gives information about the total bulk concentrations of the elements in the CNT material, the XPS method delivers results from the surface near regions of the samples.

In Table 2 the results of XPS measurements of the different CNT types, corresponding to that of Table 1, are shown. The values are calculated using standard elemental sensitivity factors and assuming a homogeneous mixture of the elements in the range of the information depth (here about 5 nm). In Figure 5 typical XP spectra of N1s and C1s are shown for the different CNT types. The C1s peaks were normalised in intensity for the peak shape comparison. CNT type C shows beside clear N corresponding peaks (for different bonding states) a broadening of the C1s line.

Correlative to the bulk chemical analysis the XP spectrum of CNT type A shows increased oxygen and the XP-spectrum of CNT type C an increased nitrogen concentration (up to 5 at% nitrogen; see Figure 5 and Table 2). A difference is found in the behaviour of the iron concentration. Whereas with the bulk analysis in all the sample types significant residuals of metal were found, XPS detected Fe only in the surface region of sample CNT type C. Obviously, the Fe particles are nearly completely embedded in the carbon tubes of type A and B. Possibly connected with the nitrogen impact, the tubes of CNT type C have a more open structure (refer also to the C1s broadening connected with surface disorder; see Figure 5) showing Fe also at the surface. A comparison of CNTs of type B and C (see HRTEM image in Figure 6) supports this assumption.

### 3.2. Electrical and morphological characterization of CNT filled PA 6.6 composites

To compare the effect of these different CNTs on the electrical properties of a polymeric matrix, all types of CNT were incorporated in polyamide 6.6 by melt mixing. The electrical conductivity values were measured on plates pressed from the melt mixed materials (Figure 7). For pure polyamide 6.6 the electrical volume conductivity was determined in earlier investigations to be $10^{-13}$ S/cm.

Polyamide 6.6 composites containing CNTs synthesised by aerosol-CVD indicate the lowest electrical percolation threshold, which was found below 0.1 wt% (Figure 7). In

this comparison, the composites containing CNTs produced using cyclohexane showed slightly higher conductivity values than those produced using acetonitrile. For polyamide filled with CNTs synthesised by fixed bed-CVD electrical percolation could be observed at CNT contents between 0.25 and 0.5 wt% (4 at% Fe), between 0.5 and 1 wt% (16 at% Fe), and between 1 and 1.5 wt% (1 at% Fe). With further increase in the CNT content the electrical volume conductivity of the composites containing fixed bed-CNTs increased slowly and the values of electrical volume conductivity were clearly lower than those of composites filled with both types of aerosol-CNTs.

In order to get an estimate for the percolation concentration $p_c$ we fitted the experimental conductivity data σ(p) for concentrations $p > p_c$ to equation:

$$\sigma(p) = B(p - p_c)^t \qquad (1)$$

which represents the well known scaling low for the composite conductivity near the electrical percolation threshold [24] The values fitted for B, pc and t using the method of the lowest value of the root mean square error are shown in Table 3. The exponents were near 2 with exception of 2.9 for the fixed bed CNT containing 4 wt% Fe in the catalyst and of x.x for the nitrogen doped multi-walled nanotubes having a bamboo-like structure. The exponent of 2 corresponds to the value applying the universal 3D lattice model [24] and the values near 3 equals to values predicted by the mean field model [25]. Interestingly, also the factor B giving a measure for the maximum conductivity is different for the composites originating from the different CVD methods. Whereas the composites made with CNT from the fixed bed method converge to values in the range of (2.2-7.5) $10^{-4}$ S/cm, the composites prepared using both aerosol methods converge to values of 0.2 S/cm which is much higher and may be assigned to the much cleaner surfaces leading to lower contact resistances in the percolated composites.

In the literature only few results concerning the electrical percolation behaviour or resistivity values of polyamide 6.6 composites were found to set our results in relation. Krause et al. [26] found for PA6.6 filled with commercially available Nanocyl® NC7000 (Nanocyl S.A., Sambreville, Belgium) melt mixed under the same conditions an electrical percolation threshold between 0.1 and 0.25 wt%. SWNT/nylon 66 composites prepared by in situ polymerization were found to be conductive starting at 2 wt% SWNT as investigated by Haggenmueller et al. [27].

Concerning polyamide 6 with a strong structural similarity to polyamide 6.6 some more results are available in literature. Meincke et al. [28] reported a percolation

concentration of 5 wt% for injection molded PA6 samples prepared using the masterbatch dilution technique starting with a 20 wt% masterbatch (Hyperion Cat. Int. Inc) using a co-rotating twin-screw extruder at a barrel temperature of 260°C [28]. Peoglos et al. [29] found an electrical percolation threshold between 2.5 wt% and 5 wt% for PA6/CNT for compression moulded plates of composites prepared from the same masterbatch using a Plasti-Corder laboratory kneader operated at 240°C, 60 rpm, and 15 min.
The results shown by Hyperion Catalysis International, Inc. (Cambridge, MA, USA) [30] indicate an electrical volume resistivity of nearly $10^4$ Ohm cm (4 wt% MWCNT) and $10^3$ Ohm cm (5 wt% MWCNT) for PA6/MWCNT composites prepared by masterbatch dilution. The electrical resistivity values of films of PA6 with 5 wt% MWCNT prepared by in situ polymerization were reported to be $3x10^5$ Ohm cm [31].

The state of nanotube dispersion was investigated using transmission light microscopy on thin sections and scanning electron microscopy on cryofractured composite surfaces. In light microscopy, remaining agglomerates with sizes above 1 µm can be observed, whereas SEM to a certain extent is also suitable to illustrate the dispersion into single tubes, their arrangement, and their complex shape in the matrix.
SEM images of the cryofractured polyamide 6.6 composites as shown in Figure 8 a-d illustrate for the composite containing aerosol-synthesised CNTs well dispersed CNT that are relatively long up to a length of 2 µm (Fig. 8 d, e). In contrast, for the polyamide filled with CNTs obtained by the fixed bed synthesis numerous areas with CNT agglomerates were observed (Fig. 8 a-c) illustrating worse CNT dispersion. In Fig. 8 b and c small white dots are visible on the sample surfaces representing broken ends of well embedded nanotubes which indicate quite good phase adhesion.
The state of macro dispersion of CNT was visualized on thin sections prepared from extruded strands using transmission light microscopy. Even if agglomerates may be embedded in the percolation structure, mostly well dispersed touching nanotubes are responsible for the formation of the percolation network. Thus the amount of dispersed tubes should be as high as possible and that of tubes remaining in agglomerates as low as possible in order to get low percolation thresholds. Interestingly, all composites filled with 1 wt% CNT exhibited CNT agglomerates with sizes larger than 5 µm (Fig. 9). This

illustrates imperfect nanotube dispersion during the melt mixing conditions applied and a remaining potential for better performing composites when obtaining better dispersion. However, the amount and size of those remaining primary agglomerates is different within the different CNT materials. Within the three different types of fixed bed-CNT (Fig. 9 a-c) the material synthesised with 4 at% Fe in the catalyst material shows the smallest summarized area of agglomerates ( 3.9±0.8 area%) as well as the smallest mean agglomerate diameter of 6.3±1.5 µm (Fig. 9b). The number of particles per $mm^2$ was determined at 1076±107. For the fixed bed-CNT containing 1 at% Fe or 16 at% Fe a summarized area of agglomerates of 9.7±1.0 area% or 5.6±0.8 area%, a mean agglomerate diameter of 16.3±4.5 µm or 24.3±3.9 µm, and a number of particle per $mm^2$ of 1438±233 or 622±40 were found. The macro dispersion of the aerosol-synthesised CNTs within the polyamide is characterized by a low amount of agglomerates and no (Fig. 9 e) or only a few (Fig. 9 d) agglomerates with small size. The summarized agglomerate area is 2.0±0.6 area% for the CNTs based on cyclohexane (Fig. 9d) and 2.0±0.5 area% for those synthesized using acetonitrile (Fig. 9e). The mean agglomerate diameter for the CNT synthesized with cyclohexane or acetonitrile was determined at 7.9±2.8 µm or 17.2±2.4 µm and the number of particles per $mm^2$ at 235±60 or 177±90. The stretched shape of the agglomerates in both samples correlates with the texture of the virgin CNT powders.

## 4. Discussion

As mentioned earlier, the correlation between synthesis condition of nanotubes, nanotube's properties, composite morphology, and electrical percolation threshold is a quite complex topic and depending on many influencing factors. Since in this paper the matrix polymer and the processing conditions of mixing and compression moulding of samples for conductivity measurements were not varied, we may concentrate on the properties of the nanotubes themselves. Main influences are their nature (SW/DW-CNT, MWCNT), their aspect ratios, their surface quality, and their dispersability behaviour in the polymer matrix based mainly on the primary agglomerate structure.

Concerning the **aspect ratio**, a high one is advantageous for the formation of a conductive CNT network at low loadings within the insulating polymer matrix. Even if a shortening of the nanotubes may be expected during melt processing, for which quantification unfortunately no reliable and fast method is available, the length of the

added nanotubes may be important for the percolation in the composites. A certain relationship may be expected between the starting length distribution and that one in the composite. In order to assess the length of the as produced CNTs, which is difficult to measure using TEM or SEM due to the scale mismatch and entanglement structure, values obtained from investigations on dispersions in aqueous surfactant solutions using a SYSMEX analysis of the different CNTs as shown in [26] were used. It was found that the aspect ratio of both CNTs synthesised using aerosol-CVD (corresponding to CNT3 and CNT4) is higher with CNT lengths partially up to 20 µm compared to the fixed bed-CNTs (CNT1, 4 at% Fe) that showed lengths shorter than 5 µm. These differences are also reflected in the SEM investigations showing much longer nanotubes on the cryofractured surfaces in case of the aerosol based CNT (Fig. 9 d, e).

The **dispersability** of the nanotube materials which is mainly determined by the entanglement structure within the as produced primary agglomerates and bundles but also by the CNT surface structure was assessed studying the sedimentation behaviour and the stability of defined prepared aqueous surfactant solutions containing the different CNTs under centrifugal forces in an analytical centrifuge LUMiFuge (L.U.M. GmbH, Berlin, Germany). These results are shown in detail in reference [26]. It was found that the dispersions of both aerosol-synthesised CNTs (CNT3, CNT4) were more stable compared to those of the fixed bed synthesised CNTs as shown in reference [26] figures 1 and 2, illustrating a better dispersability in the aqueous surfactant solutions. The dispersion of the fixed bed synthesised CNT1 (4 at% Fe) included a high fraction of big agglomerates, which settle fast. That means that the as-produced primary agglomerates during the preparation of the aqueous surfactant dispersion using ultrasonic treatment do not break up easily to individualized nanotubes. The difference in the value of individualized nanotubes was shown to illustrate the tendency of dispersability of CNTs also in polymer matrices even though the forces during ultrasonic treatment and melt mixing are not directly comparable. It is also known that more energy is required to disperse aggregated SWCNT or DWCNT in comparison to MWCNT caused by the larger surface area and interactive forces between the SWCNT/DWCNT as shown by Gojny et al. in an epoxy matrix [33].

In addition, the acid treatment step needed for the fixed-bed synthesized CNTs to remove the support material may negatively influence the dispersability of those CNT

materials. On one hand, the drying step after liquid treatment enhances the compactness of the agglomerates and thus reduces their dispersability. On the other hand, functional groups are formed at the CNT surface, as shown on enhanced oxygen content on the surface of the fixed-bed CNT, may reduce the dispersability and enhance contact resistances between touching nanotubes, both shifting the percolation concentration to higher values. This is supported by investigations of Gojny et al. [34] describing a higher electrical percolation threshold of functionalised DWCNT and MWCNT in epoxy as compared to non-functionalised CNT.

Furthermore, it was described above that the **surface** of the aerosol-synthesised CNT is very clean. Only up to 1 wt% oxygen was found at the surface using XPS measurements (table 2). Such a surface is advantageous for low contact resistances between the single nanotubes during the formation of a conductive network in the polymer matrix. Additionally, for the aerosol-CNT synthesised with cyclohexane the highest carbon content with 96.3 wt% (table 1) was found. Both effects together may be responsible for the much higher maximum conductivity level which can be achieved when using the aerosol based nanotubes in the composites (see much higher values of B in equation (1)).

The electrical percolation threshold illustrates the formation of conducting pathways trough the composite sample, thus the dispersion of the CNTs in the polymeric matrix is the link between the nanotube's properties and the electrical properties.

Interestingly, the amounts of dispersed nanotubes as estimated from the optical light microscopical images correlate as well with the results of the analysis of nanotube dispersions in aqueous solutions as with the results of electrical conductivity measurements of the composites. The two composites based on the aerosol CNTs having the better macro dispersion of the composites also showed better stability of the aqueous CNT dispersions and exhibit extremely low percolation thresholds. The composites based on CNTs synthesised by the fixed bed method containing a higher number and area of agglomerates illustrating a worse dispersability of these CNT also shown in the sedimentation results of their aqueous dispersions led to higher electrical percolation thresholds.

## 5. Summary

In our investigation, different types of CNTs were synthesised. The comprehensive characterization of these CNTs shows differences in the structure (single-, double-, multi-walled CNTs, bamboo-like or tubular) and in the chemical as well as the surface composition.

The lowest electrical percolation threshold of composites based on polyamide 6.6 prepared using the different CNT materials was observed for CNTs synthesised by the aerosol-method and used in their "as-grown state", that means without any purification, chemical treatment, or functionalisation. Here, the electrical percolation in PA6.6 was found at contents as low as 0.1 wt%, which is unusual low and not reported so far in literature for composites produced by melt mixing. The reason for this extremely low percolation threshold can be assigned to different factors. On one hand, these nanotubes possess a high aspect ratio that facilitates percolation at low contents. They also showed very stable dispersions in aqueous surfactant solutions and exhibited correspondingly a relatively good state of dispersion in the polymer matrix. On the other hand, the nanotubes produced by the aerosol method had extremely clean surfaces, showed relatively low oxygen contents near the surface, and did not show amorphous coatings, as it was the case in materials produced by the fixed bed method. This may help to reduce the contact resistance between touching nanotubes in the polymer based composites and also explains the high conductivities at low CNT loadings. This quality of a very clean surface may be also correlated to the good dispersability either in aqueous surfactant solutions or in the polymer matrix. Interestingly, the specific structures of the CNTs (bamboo-like or tubular) and connected with that the nitrogen doping only very weakly influence the electrical percolation behaviour. Both the nanotubes materials produced by the aerosol method using either acetonitrile or cyclohexane showed that low percolation threshold of lower than 0.1 wt% in PA6.6, even if the conductivity values were slightly lower for those produced using acetonitrile. In contrast, the nanotubes produced by the fixed bed method, in which a wet chemical treatment is needed in order to remove the support, exhibited lower aspect ratios, amorphous carbon coatings, and showed oxygen containing groups which in summary reduced the dispersability and resulted in higher percolation thresholds in the polyamide 6.6. Among the materials investigated, differences could be observed depending on the

amount of ferrocene in the catalyst that influenced the structure of the nanotubes synthesised.

The results clearly show that the electrical percolation behaviour is strongly dependent on the constitution of the CNTs, especially on their surface characteristics, their dispersability, as well as on the aspect ratio. The synthesis of carbon nanotubes using the aerosol method which does not need any wet treatment of the as produced material was shown to be very suitable for applications in melt mixed composites with very low electrical percolation thresholds.

**Acknowledgements**

The authors thank the Federal Ministry of Education and Research of Germany (BMBF) for the financial support within the project 03X3006.

## References


[1] Salvetat JP, Bonard JM, Thomson NH, Kulik AJ, Forro L, Benoit W, Zuppiroli L. Mechanical properties of carbon nanotubes. Applied Physics a-Materials Science & Processing 1999;69(3):255-260.

[2] Wong EW, Sheehan PE, Lieber CM. Nanobeam mechanics: Elasticity, strength, and toughness of nanorods and nanotubes. Science 1997;277(5334):1971-1975.

[3] Treacy MMJ, Ebbesen TW, Gibson JM. Exceptionally high Young's modulus observed for individual carbon nanotubes. Nature 1996;381(6584):678-680.

[4] Breuer O, Sundararaj U. Big returns from small fibers: A review of polymer/carbon nanotube composites. Polymer Composites 2004;25(6):630-645.

[5] Du J, Bai J, Cheng H. The present status and key problems of carbon nanotube based polymer composites. Polymer Letters 2007;1(5):253-273.

[6] Krause B, Pötschke P, Häußler L. Influence of small scale melt mixing conditions on electrical resistivity of carbon nanotube-polyamide composites. Composites Science and Technology 2009;69(10):1505-1515.

[7] Hernadi K, Fonseca A, Nagy JB, Bernaerts D, Lucas AA. Fe-catalyzed carbon nanotube formation. Carbon 1996;34(10):1249-1257.

[8] Colomer JF, Stephan C, Lefrant S, Van Tendeloo G, Willems I, Konya Z, Fonseca A, Laurent C, B.Nagy J. Large-scale synthesis of single-wall carbon nanotubes by catalytic chemical vapor deposition (CCVD) method. Chemical Physics Letters 2000;317(1-2):83-89.

[9] Flahaut E, Peigney A, Laurent C, Rousset A. Synthesis of single-walled carbon nanotube-Co-MgO composite powders and extraction of the nanotubes. Journal of Materials Chemistry 2000;10(2):249-252.

[10] Flahaut E, Bacsa R, Peigney A, Laurent C. Gram-scale CCVD synthesis of double-walled carbon nanotubes. Chemical Communications 2003;(12):1442-1443.

[11] Tang S, Zhong Z, Xiong Z, Sun L, Liu L, Lin J, Shen ZX, Tan KL. Controlled growth of single-walled carbon nanotubes by catalytic decomposition of CH4 over Mo/Co/MgO catalysts. Chemical Physics Letters 2001;350(1-2):19-26.

[12] Jeong HJ, Kim KK, Jeong SY, Park MH, Yang CW, Lee YH. High-yield catalytic synthesis of thin multiwalled carbon nanotubes. Journal of Physical Chemistry B 2004;108(46):17695-17698.

[13] Andrews R, Jacques D, Rao AM, Derbyshire F, Qian D, Fan X, Dickey EC, Chen J. Continuous production of aligned carbon nanotubes: a step closer to commercial realization. Chemical Physics Letters 1999;303(5-6):467-474.

[14] Mayne M, Grobert N, Terrones M, Kamalakaran R, Ruhle M, Kroto HW, Walton DRM. Pyrolytic production of aligned carbon nanotubes from homogeneously dispersed benzene-based aerosols. Chemical Physics Letters 2001;338(2-3):101-107.

[15] Kamalakaran R, Terrones M, Seeger T, Kohler-Redlich P, Ruhle M, Kim YA, Hayashi T, Endo M. Synthesis of thick and crystalline nanotube arrays by spray pyrolysis. Applied Physics Letters 2000;77(21):3385-3387.

[16] Pinault M, Mayne-L'Hermite M, Reynaud C, Beyssac O, Rouzaud JN, Clinard C. Carbon nanotubes produced by aerosol pyrolysis: growth mechanisms and post-annealing effects. Diamond and Related Materials 2004;13(4-8):1266-1269.

[17] Vivekchand SRC, Cele LM, Deepak FL, Raju AR, Govindaraj A. Carbon nanotubes by nebulized spray pyrolysis. Chemical Physics Letters 2004;386(4-6):313-318.

[18] Coquay P, Peigney A, De Grave E, Flahaut E, Vandenberghe RE, Laurent C. Fe/Co alloys for the catalytic chemical vapor deposition synthesis of single- and double-walled carbon nanotubes (CNTs). 1. The CNT-Fe/Co-MgO system. Journal of Physical Chemistry B 2005;109(38):17813-17824.
[19] Patil KC. Advanced Ceramics - Combustion Synthesis and Properties. Bulletin of Materials Science 1993;16(6):533-541.
[20] Datsyuk V, Kalyva M, Papagelis K, Parthenios J, Tasis D, Siokou A, Kallitsis I, Galiotis C. Chemical oxidation of multiwalled carbon nanotubes. Carbon 2008;46(6):833-840.
[21] Terrones M, Terrones H, Grobert N, Hsu WK, Zhu YQ, Hare JP, Kroto HW, Walton DRM, Kohler-Redlich P, Ruhle M, Zhang JP, Cheetham AK. Efficient route to large arrays of CNx nanofibers by pyrolysis of ferrocene/melamine mixtures. Applied Physics Letters 1999;75(25):3932-3934.
[22] Glerup M, Castignolles M, Holzinger M, Hug G, Loiseau A, Bernier P. Synthesis of highly nitrogen-doped multi-walled carbon nanotubes. Chemical Communications 2003;(20):2542-2543.
[23] Tang C, Bando Y, Golberg D, Xu F. Structure and nitrogen incorporation of carbon nanotubes synthesized by catalytic pyrolysis of dimethylformamide. Carbon 2004;42(12-13):2625-2633.
[24] Stauffer D, Aharony A. Introduction in percolation theory. London: Taylor and Francis, 1994.
[25] Heaney MB. Measurement and interpretation of nonuniversal critical exponents in disordered conductor–insulator composites. Physical Review B 1995;52(17):12477.
[26] Krause B, Petzold G, Pegel S, Pötschke P. Correlation of carbon nanotube dispersability in aqueous surfactant solutions and polymers. Carbon 2009;47(3):602-612.
[27] Haggenmueller R, Du F, Fischer JE, Winey KI. Interfacial in situ polymerization of single wall carbon nanotube/nylon 6,6 nanocomposites. Polymer 2006;47(7):2381-2388.
[28] Meincke O, Kaempfer D, Weickmann H, Friedrich C, Vathauer M, Warth H. Mechanical properties and electrical conductivity of carbon-nanotube filled polyamide-6 and its blends with acrylonitrile/butadiene/styrene. Polymer 2004;45(3):739-748.
[29] Peoglos V, Logakis E, Pandis C, Pissis P, Pionteck J, Pötschke P, Micusik M, Omastova M. Thermal and electrical characterization of multi-walled carbon nanotubes reinforced polyamide 6 nanocomposites. Journal of Nanostructured Polymers and Nanocomposites 2007;3(4):116-124.
[30] http://www.fibrils.com/PDFs/perc%20curve-crystalline.pdf (assessed May 19th 2009) "Electrical Resistivity in Semi-Crystalline Polymers as a Function of FIBRIL™ Nanotube Loadings".
[31] Saeed K, Park SY. Preparation of multiwalled carbon nanotube/nylon-6 nanocomposites by in situ polymerization. Journal of Applied Polymer Science 2007;106(6):3729-3735.
[32] Kasaliwal G, Göldel A, Pötschke P. Influence of processing conditions in small-scale melt mixing and compression molding on the resistivity and morphology of polycarbonate-MWNT composites. Journal of Applied Polymer Science 2009;112(6):3494-3509.
[33] Gojny FH, Wichmann MHG, Fiedler B, Schulte K. Influence of different carbon nanotubes on the mechanical properties of epoxy matrix composites - A comparative study. Composites Science and Technology 2005;65(15-16):2300-2313.
[34] Gojny FH, Wichmann MHG, Fiedler B, Kinloch IA, Bauhofer W, Windle AH, Schulte K. Evaluation and identification of electrical and thermal conduction

**mechanisms in carbon nanotube/epoxy composites. Polymer 2006;47(6):2036-2045.**

**Figure Captions**

Figure 1: HRTEM micrograph of individual CNT (a) MWCNT grown by the fixed bed method (16 at% Fe) ; (b)MWCNT and (c) DWCNT grown on the reduction product with 4 at% Fe.

Figure 2: HRTEM micrograph of CNTs grown on the reduction product with 1 at% Fe; (a) individual DWCNTs with an outer diameter of approx. 3nm and (b) bundles of DW/SWCNTs

Figure 3: TEM image of MWCNTs deposited by the aerosol-CVD (a) with cyclohexane and (b) acetonitrile.

Figure 4: Diameter distribution histogram of MWCNTs deposited by the aerosol-CVD using (a) cyclohexane and (b) acetonitrile

Figure 5: (a) N1s and (b) C1s spectra of the three different CNT types; A: fixed bed-CNTs (4 at% Fe), B: aerosol-CNTs with cyclohexane as solvent; C: aerosol-CNTs with acetonitrile as solvent.

Figure 6: Typical HRTEM image of MWCNT with an iron catalyst particle. Left: in the middle of the tube, aerosol-CVD with cyclohexane (type B); Right: at an end of the tube, aerosol-CVD with acetonitrile (type C).

Figure 7: Electrical conductivity of polyamide 6.6 composites containing different CNT.

Figure 8: SEM images of cryofracted PA6.6 composites containing 1 wt% CNT: (a) fixed bed-CNTs with 1 at% Fe; (b) fixed bed-CNTs with 4 at% Fe (type A); (c) fixed bed-CNTs with 16 at% Fe; (d) aerosol-CVD with cyclohexane (type B); (e) aerosol-CVD with acetonitrile (type C).

Figure 9: Light microscopy images of PA6.6 composites containing 1 wt% CNT: (a) fixed bed-CNTs with 1 at% Fe; (b) fixed bed-CNTs with 4 at% Fe (type A); (c) fixed bed-CNTs with 16 at% Fe; (d) aerosol-CVD with cyclohexane (type B); (e) aerosol-CVD with acetonitrile (type C).

Tables

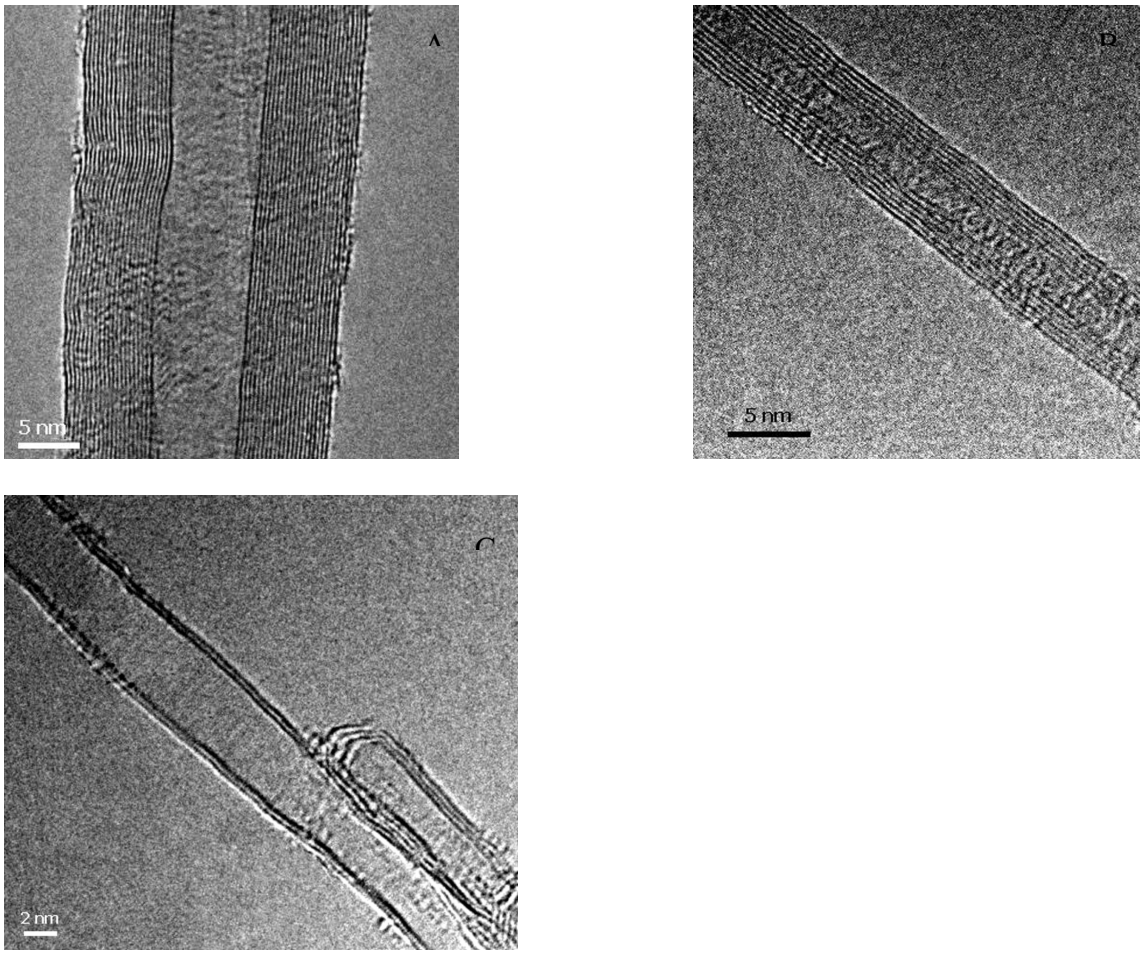


Figure 1

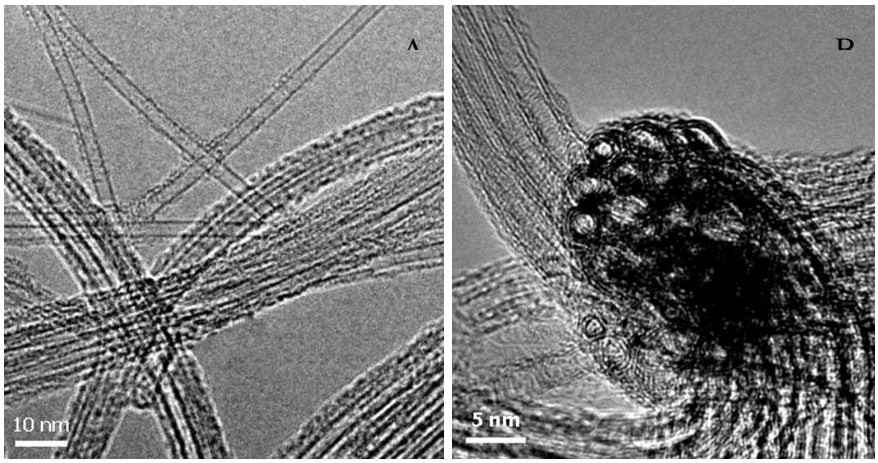


Figure 2

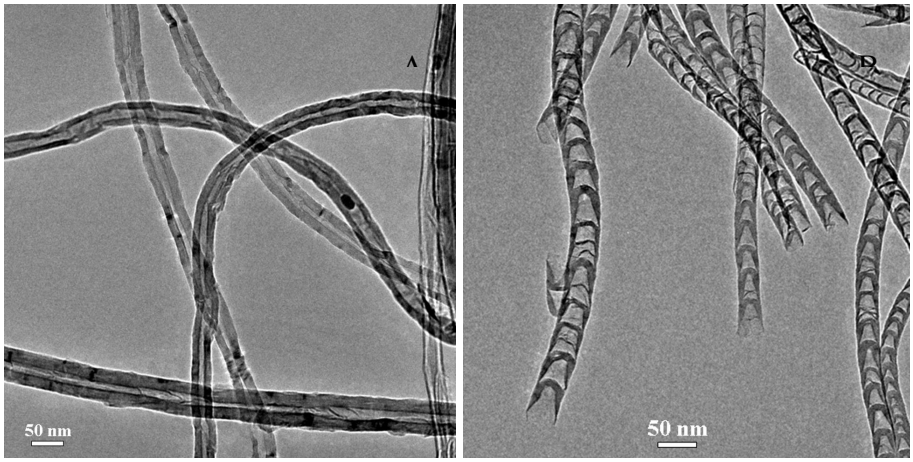


Figure 3

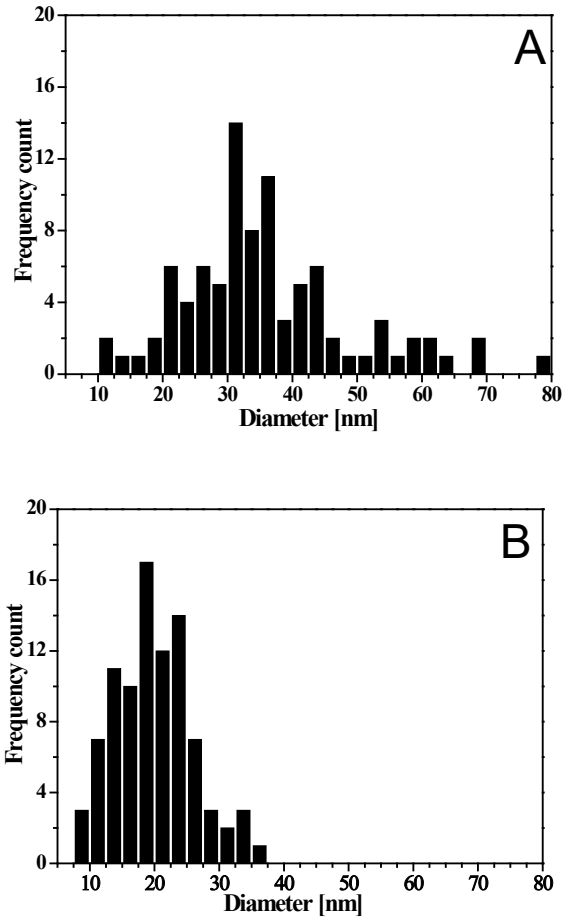


Figure 4

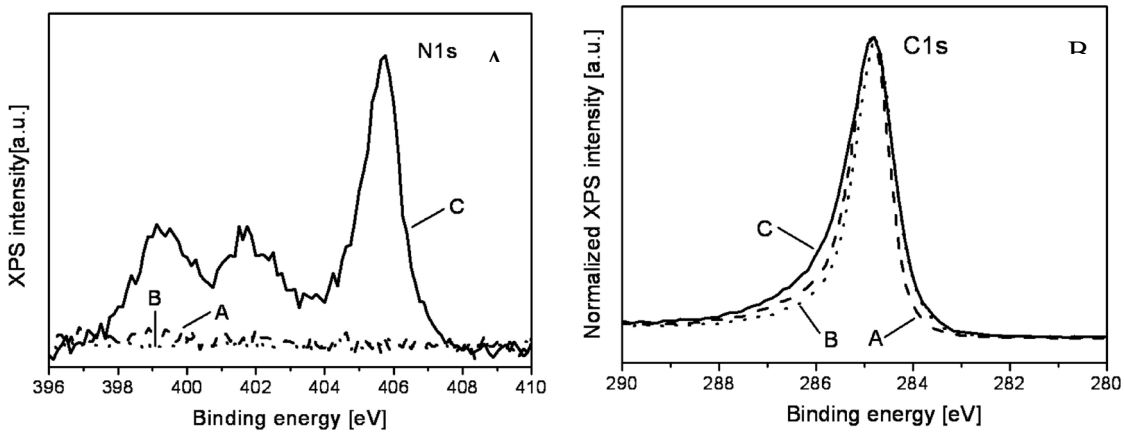


Figure 5

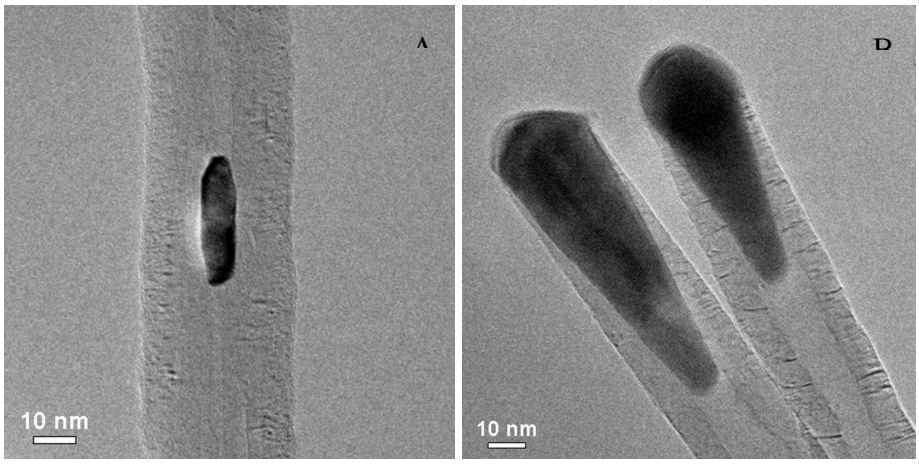


Figure 6

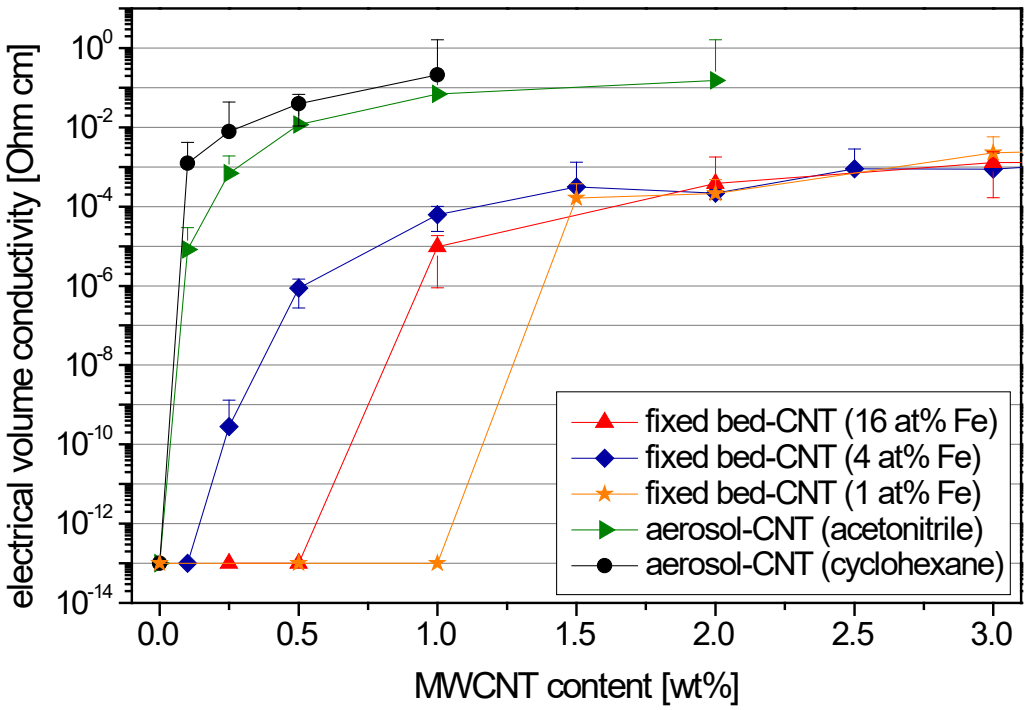
electrical volume conductivity [Ohm cm]
10^0
10^-2
10^-4
10^-6
10^-8
10^-10
10^-12
10^-14
0.0
0.5
1.0
1.5
2.0
2.5
3.0
MWCNT content [wt%]
fixed bed-CNT (16 at% Fe)
fixed bed-CNT (4 at% Fe)
fixed bed-CNT (1 at% Fe)
aerosol-CNT (acetonitrile)
aerosol-CNT (cyclohexane)

Figure 7

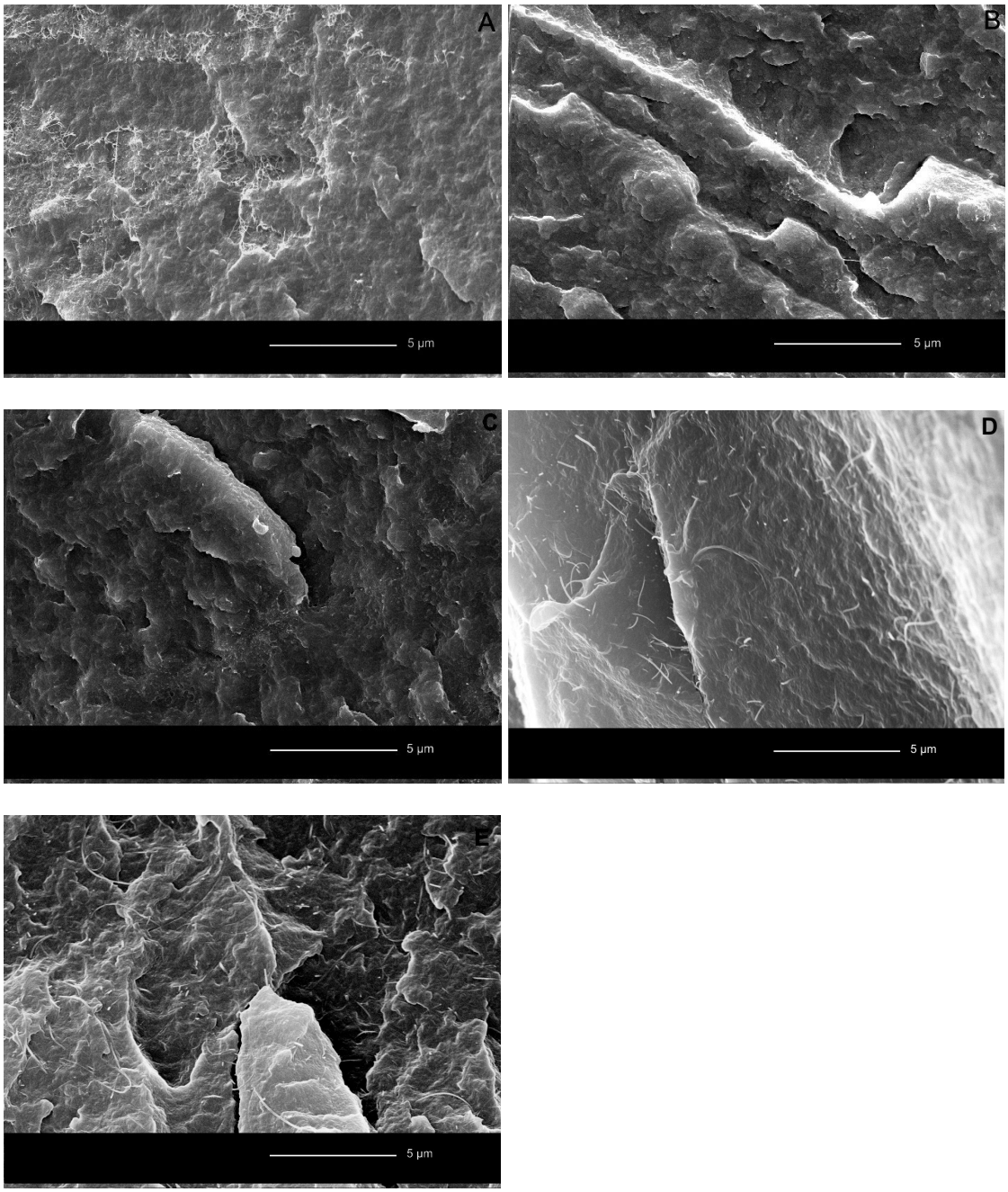


Figure 8

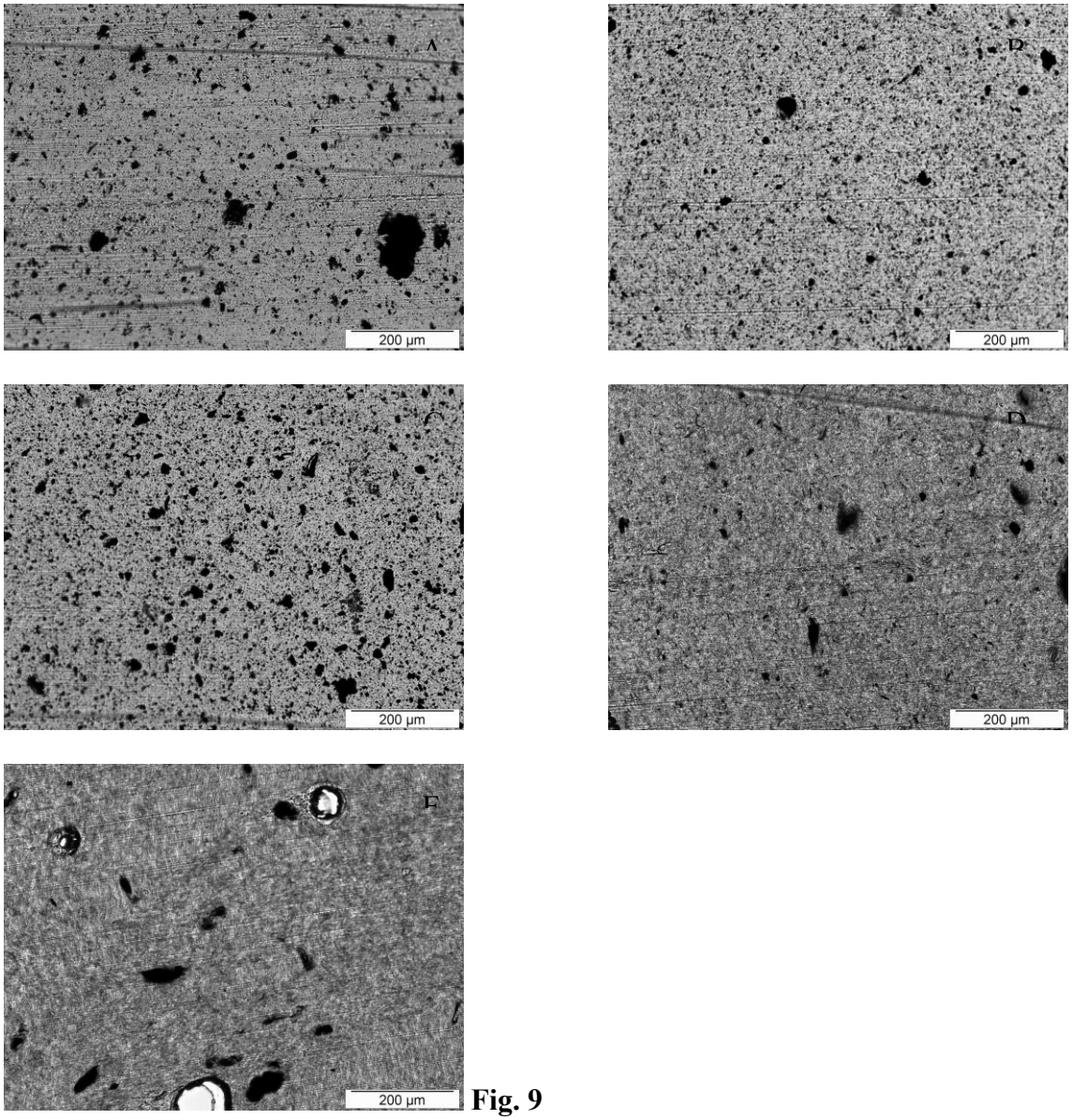


**Fig. 9**

Tables

Table 1

Chemical composition of applied CNT types

| CNT type | C [wt%] | O [wt%] | N [wt%] | Fe* [wt%] | H [wt%] | Sum [wt%] |
|---|---|---|---|---|---|---|
| A | 89.4 | 2.60 | 0.270 | 5.60 | 0.391 | 98.8 |
| B | 96.3 | 0.17 | 0.046 | 2.56 | 0.250 | 99.3 |
| C | 86.2 | 0.48 | 11.200 | 2.40 | 0.140 | 100.4 |

*(+Mo: 6.25 wt%)

Table 2

Surface compositions of the CNT types determined by XPS (normalized to 100%)

| CNT type | C [wt%] | O [wt%] | N [wt%] | Fe [wt%] |
|---|---|---|---|---|
| A | 97.05 | 2.38 | 0.11 | 0.46 |
| B | 98.32 | 1.06 | 0.16 | 0.46 |
| C | 89.22 | 0.76 | 5.57 | 4.45 |

Table 3

Results of the curve fitting procedure of conductivity values for $p>p_c$

| sample | B [S/cm] | t | percolation concentration $p_c$ [wt%] |
|---|---|---|---|
| fixed bed-CNT (16% at% Fe) | 2.6E-4 | 2.1 | 0.63 |
| fixed bed-CNT (4% at% Fe), Type A | 2.2E-4 | 2.9 | 0.35 |
| fixed bed-CNT (1 at% Fe) | 7.5E-4 | 2.0 | 1.03 |
| aerosol-CNT (cyclohexane), Type B | 0.19 | 2.0 | 0.04 |
| aerosol-CNT (acetonitrile), Type C | 0.19 | 3.6 | 0.04 |